A Multimodal Twisted-Winching String Actuator with a Passive Automatic Transmission: Design and Validation

Author 1*, Author 2*, and Author 3

***Abstract*— This paper presents a novel single-motor actuator that integrates a twisted string actuator (TSA) and a winch mechanism with passive automatic clutches. This approach enables seamless transitions from large displacement winching to high force twisting without additional motors. The actuator leverages the characteristics of its epicylic-style gear transmission system to passively transition from high displacement winching to high force twisting when the load on the string exceeds a force threshold. A slip clutch integrated with a unidirectional bearing ensures complete untwist and unwinch cycles, returning the system to its original state. A mechanical dial with a high-reduction gearbox permanently encodes the system's twisted state, ensuring precise and repeatable untwisting cycles. Mathematical models characterize the clutch torque thresholds, force output, and string kinematics. Experimental validation demonstrates the actuator's ability to achieve efficient, reliable transitions and force amplification. This design eliminates the need for additional motors and simplifies control. It offers a compact, efficient solution for tendon-driven robotic applications, specifically those that require large initial displacements followed by high force outputs.**

I. INTRODUCTION

Prosthetics, surgical robots, and collaborative robots require actuators that combine force, speed, dexterity, and compact size. Traditional actuators often excel in one aspect at the expense of others. Electric motors with gearboxes, while capable, can often be bulky and inefficient. Hydraulic and pneumatic systems deliver high power but lack the miniaturization needed for precise, dexterous applications. This trade-off motivates the development of alternative actuation technologies that prioritize compactness, efficiency, and versatility across a wide operational range.

Twisted string actuators (TSAs) present a promising alternative by converting rotational motion into linear displacement through string twisting. TSAs achieve high transmission ratios without the weight and complexity associated with traditional gearboxes [1], [2]. Their lightweight and compact nature makes them particularly attractive for applications with stringent spatial constraints but high force demands [3], [4]. However, TSAs inherently suffer from limited stroke length and fixed force transmission ratios, which restrict their overall versatility [5], [6].

Winch-based actuators, by contrast, offer greater displacement capabilities but with reduced force output [7]. To leverage the advantages of both TSA and winch mechanisms, hybrid approaches have emerged. Previous works utilized dual-motor systems, employing winch mechanisms for large displacements and TSA mechanisms for high-force applications [8]. An alternative design aligned the motor, winch, and string along a single axis and employed a dog clutch to switch between twisting and winching modes [9], [10], [11]. However, high friction during the twisting phase prevented simultaneous mode operation and limited precise control over both the string's rotational and linear states.

The reliance on an additional motor in these designs, whether for clutch actuation or enhanced string control, introduces complexities in control strategies and can increase the overall system size. Especially for common use cases

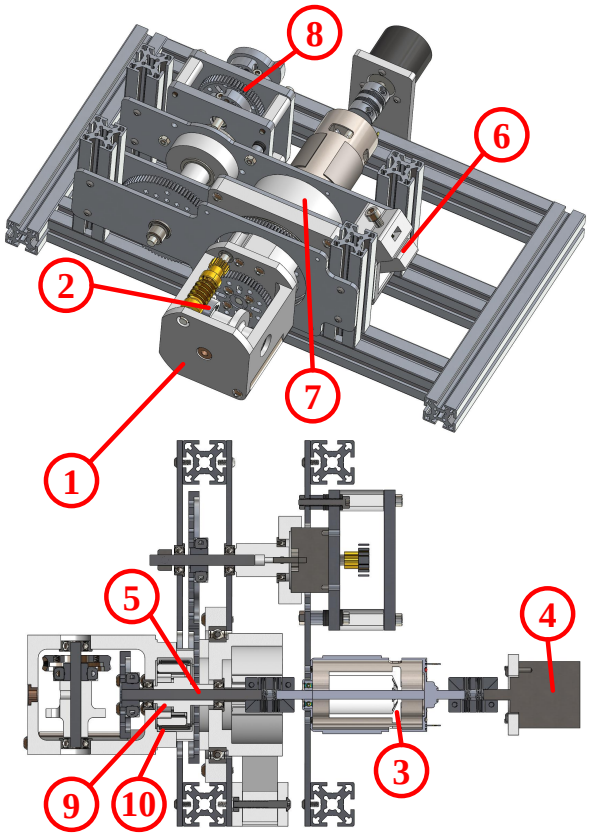

Fig. 1. The TSA/winch hybrid actuator. The turret (1) houses the worm gear assembly and winch (2). The actuator is driven by a brushed motor (3) with an encoder (4) via a through-hole drive shaft (5). Rotational friction can be adjusted via the cantilever beam contact (6) pressed against the turret ring (7). After the winching phase, the subsequent twisting rotations are mechanically recorded by a high-reduction gearbox (8). During the reverse direction (untwisting), a dial on this gearbox hits a mechanical stop, after which an integrated slip clutch (9) and unidirectional bearing (10) enable the system to fully unwind to its original state.

*These authors contributed equally to this work.

The authors are with the [lab], [university], [location] (email: email 1; email 2; email 3)

where an actuator needs to rapidly reach a position before applying a high force, a simpler and more efficient single-motor solution is highly desirable. Several efforts have attempted to replace the extra motor with a passive element. One such design substituted the actuated clutch with a passive friction slip clutch, activating the twisting mode when the torque exceeded a predefined threshold [5], [12]. However, the reverse action was load-dependent, potentially preventing a complete untwist and unwinch if the load suddenly disappeared. Consequently, for applications requiring the actuator to reliably return to its initial state before the next operation (e.g., in a pick-and-place tendon-driven hand), the design proposed in [5], [12] was insufficient.

String actuators that returned to their initial state after a contraction cycle regardless of the antagonist load have been done before but came with their own set of disadvantages. One actuator used a tapered pulley design where a spring-loaded stage shifted the string to a section with a smaller radius when the string encountered a higher load, increasing the force output of the pulley [13]. Another actuator used a pinion and a spring-loaded rack such that when the load at the end of the string increased, the rack was pulled in to contact the pinion and increase the force output [14]. Both allowed complete unwinding, but both do not exploit the high force potential of string twisting. As a result, they were unable to control the force output without redesigning the mechanism.

This work presents an actuator that replaces the motor seen in [8] with several mechanisms. It merges the advantages of winching and twisting into a single-motor driven unit. An automatic friction clutch, inspired by planetary gearbox mechanics and triggered by a high end-effector load, allows the actuator to transition from winching to twisting, maximizing force output according to the user's desired number of rotations. This number of rotations is mechanically stored using a dial on the output shaft of a high-reduction gearbox. Furthermore, a slip clutch integrated with a unidirectional bearing enables complete untwisting and unwinching, ensuring the actuator can reliably return to its starting configuration. Detailed explanations of these mechanisms are illustrated in Section II and Fig. 2.

This hybrid TSA-winch actuator design presents a novel advancement by eliminating the need for multiple motors. While it sacrifices direct control over the string's rotational and linear states at all times, its design excels in scenarios demanding high force application after rapid initial movement. The key contributions of this paper are:

1) A novel twisted-winching string actuator design that collectively features a single motor drive, a passive automatic clutch to switch between high force twisting and high displacement winching, and the ability to return the string to its initial state.
2) Mathematical models and methods to tune the torque thresholds of the clutches both in the forward and reverse directions for any similar design.
3) Experimental results that validate said models and demonstrate the viability of said actuator.

This paper presents the design of this novel actuator, the mathematical models for its operation, and finally its performance in experiments. Our aim is to provide an efficient and versatile actuation system that autonomously adapts to load demands, suitable for advanced robotic applications where space and weight are critical constraints.

II. DESIGN

A. Actuator Forward Mechanism

The actuator initiates operation with a winching phase, where the motor's rotation is transmitted via a through-hole driveshaft (Fig. 1, part 5) to a worm gear assembly. A slip clutch is mounted directly on the driveshaft and is housed inside a unidirectional roller bearing. This bearing is oriented to allow free rotation of the driveshaft without turret rotation during winching.

An increasing load on the string passively triggers the transition from winching to twisting. The gear transmission in the turret resembles a planetary gear system, where the "sun" gear corresponds to the gear on the driveshaft, the "planet" gear connects to the worm gear, and the turret acts as the "planetary carrier" (Fig. 3). Under high resistive load at the end of the string, the planetary gear is effectively locked through the worm gear, causing the motor's torque to rotate the planetary carrier turret directly at the same speed of the sun gear (Step 2 of Fig. 2) and thereby twisting the string. The sharp reduction in motor current provides a clear signal that the winching phase has concluded, enabling the identification of the necessary rotations for complete unwinching. Subsequently, this entire assembly will be referred to as the "friction clutch."

The following turret rotations must overcome the frictional resistance generated by an adjustable cantilever beam contact pressed against the turret ring (Fig. 1, parts 6 and 7). This mechanism allows for fine-tuning of the string force threshold required for this transition, enabling precise load-dependent engagement of the twisting mode. The number of turret rotations is mechanically recorded by a high-reduction (76:1) gearbox connected to a dial (Fig. 1, part 8). As the turret rotates to twist the string, this dial turns away from a fixed hard stop. This dial thus tracks the rotations, ensuring consistent and repeatable operation.

B. Actuator Reverse Mechanism

In the reverse direction, the motor untwists the string by directly rotating the turret in the opposite direction via the unidirectional roller bearing. Once the gearbox dial reaches its hard stop, the slip clutch within the unidirectional roller bearing engages, allowing the driveshaft to continue rotating independently of the turret. This, in conjunction with the rotational position recorded by the motor encoder during the sharp current shift at the forward transition threshold, ensures complete unwinching of the string to its original state. The slip clutch incorporates curved flexure detents that deform under sufficient torque, enabling controlled slippage. The torque required to activate the slip clutch is designed to

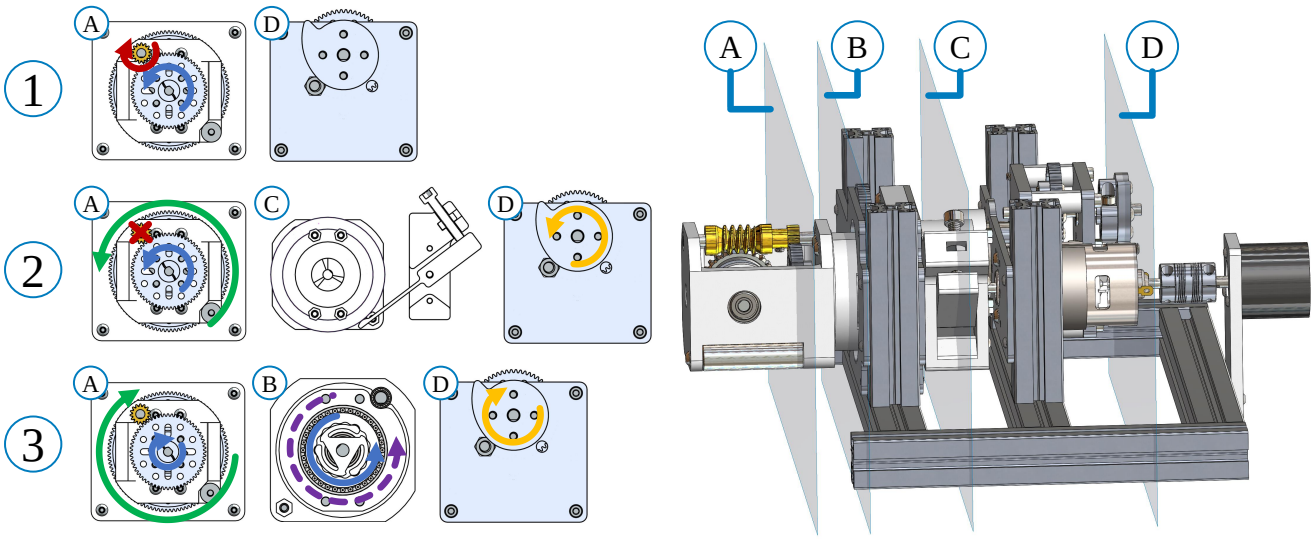

Fig. 2. Operation process flow with cross sections of the turret gear system (A), slip clutch and unidirectional roller bearing (B), cantilever beam contact (C), and gearbox dial (D). Step 1: The "sun" gear rotates (blue arrow) via the driveshaft, rotating the "planet" and worm gears to wind the string. Step 2: Increased string load locks the "planet" gear, redirecting motor torque to the turret (green arrow) and string twisting. Rotational friction can be adjusted via the cantilever contact (C), and turret rotation turns the gearbox dial away from a hard stop (orange arrow). Step 3: Motor reverses direction to untwist. Torque is transmitted via a unidirectional bearing oriented such that the turret rotates first (purple arrow), allowing pure untwisting until dial hits the hard stop. The slip clutch inside unidirectional bearing then begins to slip, allowing pure unwinching.

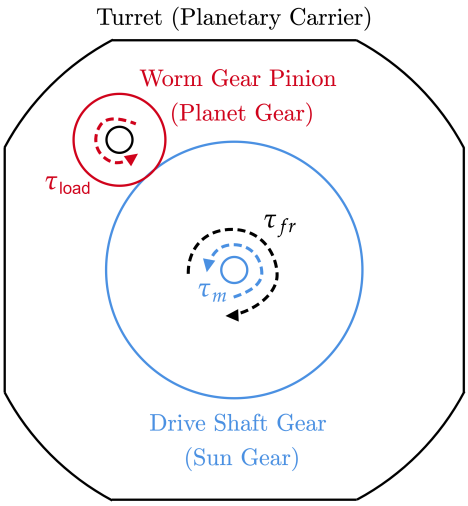

Fig. 3. Diagram of turret gearing that acts as a friction clutch, analogous to a planetary gearing system. The gears are labeled as part 2 in Fig. 1.

ensure smooth operation without exceeding the mechanical limits of the unidirectional bearing or the gearbox.

III. MODELS AND EQUATIONS

A. Friction Clutch Modeling

The friction clutch that allows the actuator to switch from winching to twisting depends on the interplay between the load force at the end effector on the string F, the rotational friction of the turret τ_{fr}, and the torque applied by the motor τ_m. As mentioned before, the turret and gearing assembly resembles a planetary gearbox with a sun gear, planet gear, and planetary carrier (Fig. 3). The elements rotate about each other in manners dependent on the torques on each of these elements. In order for the design proposed in this work to winch first and then twist,

$$0 < \tau_{\text{load}} < \tau_{fr} < \tau_{m,\max}, \tag{1}$$

where τ_{load} can be perceived as the resistive torque caused by the load F, and $\tau_{m,\max}$ is the maximum possible torque supplied by the motor.

This relationship in Equation 1 is enforced through the design of the actuator and ensures that the actuator does not exhibit some unwanted behaviors. If $\tau_{fr} < \tau_{\text{load}}$, simultaneous twisting and winching can occur. If $\tau_{\text{load}} < \tau_{m,\max} < \tau_{fr}$ or $\tau_{m,\max} < \tau_{\text{load}} < \tau_{fr}$, stalling in the winching phase before twisting can occur. While the dynamics dictating the motion of the actuator under the condition $\tau_{fr} < \tau_{\text{load}}$ are interesting, they will not be studied here.

The torque τ_{load} is interpreted as a resistive load because of the non-backdrivability of the worm gear assembly. Even if F becomes infinitely large, it can cause no rotational movement of the sun gear in the reverse direction. In this way (and under the condition in Equation 1), τ_{load} can be mathematically represented as

$$\tau_{\text{load}} = \begin{cases} \frac{Fr_w}{N_{\text{worm}}} & \text{if } \frac{Fr_w}{N_{\text{worm}}} < \tau_m \\ \tau_m & \text{if } \frac{Fr_w}{N_{\text{worm}}} \geq \tau_m \end{cases}, \tag{2}$$

where r_w is the radius of the winch and N_{worm} is the gear reduction across the worm gear. It should be noted that Equation 2 is a piecewise function—F causes an increase in the resistive torque opposing τ_m until there isn't enough

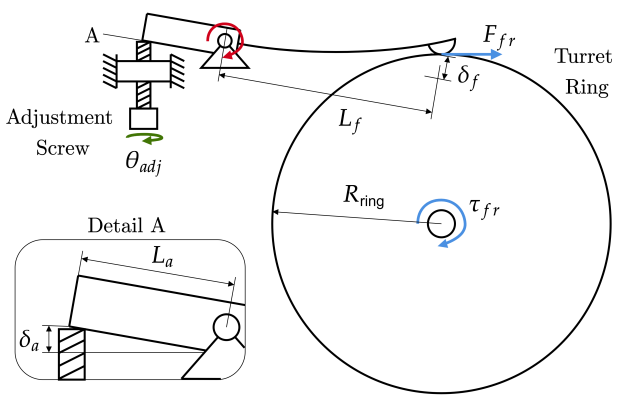

Fig. 4. Diagram of the spring-loaded contact against the turret ring that can be tuned to adjust τ_{fr}.

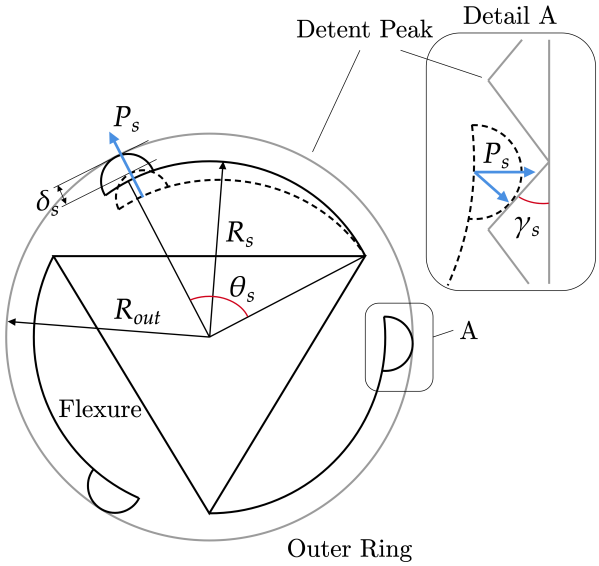

Fig. 5. Diagram of the slip clutch flexures and outer ring geometry.

motor torque to overcome it. At this point, the planet gear is effectively held rigid, $\tau_{\text{load}} = \tau_m$. All motor torque is transmitted directly to the planetary carrier turret to overcome τ_{fr}. Because $\tau_{\text{load}} < \tau_{fr}$ as established by Equation 1 and enforced by the design, the planetary carrier turret rotating while the planet gear rotates is not a concern.

The rotational friction τ_{fr} resisting the motion of the turret assumes that bearing friction is negligible and is dependent on the adjustable contact that is pressed against the turret ring (Fig. 4). This contact is mounted at the end of a cantilever beam. When the base of the beam is tilted (Point A in Fig. 4) by means of turning the adjustment screw, the cantilever beam bends, exerting an elastic force on the surface of the turret ring and increasing rotational friction. Hence, the rotational friction is

$$\tau_{fr} = \mu_f R_{\text{ring}} \frac{E_f I_f \delta_f}{L_f^3}, \tag{3}$$

where μ_f is the friction coefficient between the beam and the turret ring, R_{ring} is the outer radius of the ring, E_f is the elasticity modulus of the beam material, $I_f = \frac{1}{12} b_f h_f^3$ is the second moment of area, and L_f is the length of the beam (Fig. 4). The deflection δ_f at the end of the beam depends on the number of turns of the adjustment screw θ_{adj},

$$\delta_f \approx L_f \tan\left(\sin^{-1}\left(\frac{\theta_{\text{adj}} p_{\text{adj}}}{L_a}\right)\right), \tag{4}$$

where p_{adj} is the pitch of said screw and L_a is the dimension seen in Detail A of Fig. 4.

By design of the beam and by turning the adjustment screw, τ_{fr} can be tuned to ensure that Equation 1 holds true. The greater that τ_{fr} increases, the higher that τ_{load} can be, but stalling will occur if τ_{fr} exceeds the maximum deliverable torque of the motor. Furthermore, the rotational acceleration of the turret α depends on τ_{fr},

$$\alpha = \frac{\tau_m - \tau_{fr}}{I}, \tag{5}$$

where I is the turret's moment of inertia. Hence, if it is desired that the turret achieves a particular acceleration, it is important to consider the effects of τ_{fr}—which will always be present while the turret turns—on α when tuning.

B. Reverse Direction Slip Clutch

Once the dial at the end of the gearbox hits the hard stop, the clutch inside the unidirectional roller bearing should begin to slip. The amount of torque required to cause slip τ_s is related to the curved flexures of the clutch bending out of the detent and the friction,

$$\begin{aligned} \tau_s &= 3(P_s \mu_s \cos(\gamma_s) + P_s \sin(\gamma_s)) \cos(\gamma_s) R_{\text{out}}, \\ P_s &= \frac{4 E_s I_s \delta_s}{R_s^3 (2\theta_s - \sin(2\theta_s))}, \end{aligned} \tag{6}$$

where P_s is the elastic force of the flexure as it is deformed while slipping, μ_s is the friction coefficient between the flexure tip and the outer ring, E_s is the elasticity modulus of the flexure beam, $I_s = \frac{1}{12} b_s h_s^3$ is the second moment of area of said beam, δ_s is the beam tip displacement, and θ_s is the angular span of the curved beam flexure (Fig. 5). Equation 6, derived using Castigliano's method for curved beams and a trigonometric identity for $\sin^2(x)$, assumes that the detents on the outer ring are simple ramps with angle γ_s as seen in Detail A of Fig. 5. R_{out} is the radial distance from the axial center of the clutch to the peak of the detent, where δ_s and P_s are expected to be greatest. The first and second terms in the parentheses are the forces required to overcome friction and the flexure spring force, respectively.

Some conditions must be met in order for the reverse direction procedure to run as intended. Firstly, to ensure that stalling does not occur,

$$\tau_s + \tau_{\text{ant}} + \tau_{fr} < \tau_{m,\max}, \tag{7}$$

where τ_{ant} is the resistive torque caused by the antagonist force acting at the end of the string. In most tendon-driven mechanisms, this often takes the form of a passive elastic element like a spring that keeps the string taut and allows the driven element to return to its original position when the actuator does not exert force. Here, τ_{ant} has the same direction as τ_{load} in Fig. 3. Additionally,

$$\tau_{\text{ant}} + \tau_s > \tau_{fr}. \tag{8}$$

If the condition in Equation 8 does not hold true but Equation 7 does, unwinching will occur before any untwisting, which is undesirable. For example, if $\tau_s < \tau_{fr}$, τ_{ant} cannot be zero—there must be some antagonist force to prevent unwinching from occurring before completely untwisting.

It should also be noted that the torque required to trigger the slip clutch τ_s should be less than the torque limit of the unidirectional roller bearing and the torque limit of the gearbox teeth, $\tau_s < \tau_{\text{bearing}}$ and $\tau_s < \tau_{\text{gear}}$. Both τ_{bearing} and τ_{gear} can be typically found from the vendor.

C. String Modeling

Because the winching and twisting modes occur sequentially rather than simultaneously, the total contraction of the string ΔX can be described as a piecewise function of the separate displacements during winching and twisting:

$$\Delta X = \begin{cases} \Delta X_{\text{winch}} & \text{if } \tau_m > \tau_{\text{load}} \\ \Delta X_{\text{twist}} & \text{if } \tau_m \leq \tau_{\text{load}} \end{cases}, \tag{9}$$

where ΔX_{winch} is the displacement due to winching before the transition, and ΔX_{twist} is the displacement due to the following twisting action. The winch displacement contribution ΔX_{winch} is

$$\Delta X_{\text{winch}} = \frac{r_w \phi}{N_{\text{winch}}}, \tag{10}$$

where r_w is the radius of the winch drum, ϕ is the rotation angle of the motor, and N_{winch} is the gear reduction between the motor and the winch. When the actuator enters the twisting phase, the displacement due to twisting is:

$$\Delta X_{\text{twist}} = L_c - \sqrt{L_c^2 - (\phi r_0)^2}, \tag{11}$$

where L_c is the contracted length of the string and r_0 is the initial radius of the string. The contracted length of the string L_c can be described as $L - r_w \phi_w$, with L being the original resting length of the string and ϕ_w being the number of rotations at the end of the winching phase.

Models for the linear velocity of the string end effector can be found by taking the time derivatives of Equations 10 and 11. Before the transition to twisting, the linear velocity due to the winching action is

$$\dot{X}_{\text{winch}} = r_w \dot{\phi}, \tag{12}$$

and that during the twisting phase is

$$\dot{X}_{\text{twist}} = -\frac{\phi r_0^2 \dot{\phi}}{\sqrt{L_c^2 - (\phi r_0)^2}}. \tag{13}$$

The total linear velocity $\dot{X}$ can hence be described as

$$\dot{X} = \begin{cases} \dot{X}_{\text{winch}} & \text{if } \tau_m > \tau_{\text{load}} \\ \dot{X}_{\text{twist}} & \text{if } \tau_m \leq \tau_{\text{load}} \end{cases}. \tag{14}$$

D. Force Output

As expected, the force outputs of the winching and twisting phase are different and are replicated here from [8] for completeness. During the winching phase, the force output F_{winch} is

$$F_{\text{winch}} = \frac{\tau_m N_{\text{winch}}}{r_w}. \tag{15}$$

The force from twisting action F_{twist} is

$$F_{\text{twist}} = K\left(\sqrt{L_c^2 + \phi^2 r_0^2} - L_c\right)\cos(\beta) \tag{16}$$

where K is the stiffness of the string and β is the helix angle of the string as it twists. The force output with respect to motor current draw during twisting can be significantly higher past a certain ϕ due to the mechanical advantage provided by the twisting mechanism.

IV. EXPERIMENTAL SETUP AND CALIBRATION

The experimental setup seen in Fig. 6 consisted of a 775 brushed motor coupled to the actuator. The string comprised of four 0.8 mm diameter UHMWPE cords because of high material stiffness and better adherence to models due to the resulting stranded structure [8]. This string was wound about the winch, which was manipulated according to the design described in Section II. The string end was tied to the clevis of a pneumatic cylinder with a 32 mm bore, 200 mm stroke, and measured sliding friction force of 12.45 N.

Measurement and driving electronics were built around the modular microcontroller infrastructure offered by TinkerForge. A DC Bricklet 2.0 ran the brushed motor, and an Industrial Counter Bricklet was used for motor encoder readings. Everything was powered by a 24V power supply, with the drawn current being measured by a Voltage/Current Bricklet 2.0. For driving the cylinder (Fig. 7), a Festo MHE3 3/2 valve was used to vent the cylinder to atmospheric pressure (P_0). When pressurized, a Festo VEAB piezo pressure regulator was employed to add pressure to the cylinder. The pressure (P_1) could be dynamically adjusted to provide variable force F_c to the actuator. The built-in pressure sensor of the regulator was used to verify the commanded pressure. The setpoint voltage was set using an Industrial Analog Out Bricklet, while the pressure was read via an Industrial Dual Analog In Bricklet. The cylinder rod was linked to the stage of a P3 America OPH Series linear potentiometer running parallel to the cylinder stroke and measuring string displacement via a Dual Analog-In Bricklet.

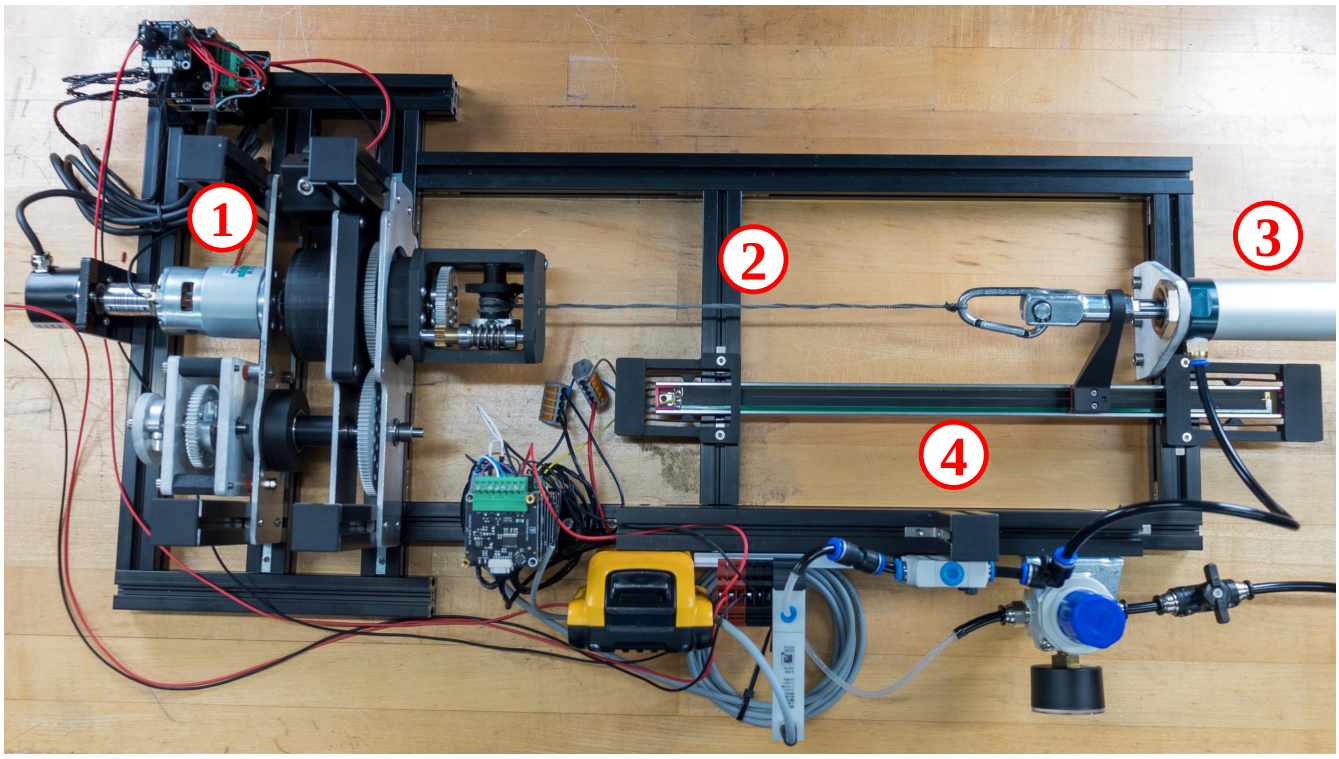

Fig. 6. The experimental setup. The actuator (1) manipulates the string (2), which is attached to a pneumatic cylinder (3). The cylinder head is attached to a linear potentiometer (4).

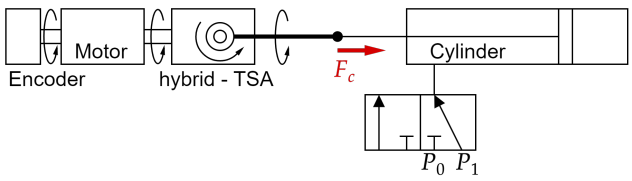

Fig. 7. Pneumatic system layout with valves.

N_{worm}	r_w [mm]	F [N]	L_f [mm]
28	9	30	50
θ_{adj} [rad]	p_{adj} [mm/rad]	L_a [mm]	μ_f
18.87	0.16	28.23	0.28
E_f [GPa]	b_f [mm]	h_f [mm]	μ_s
2.0	20	2	0.28
γ_s [rad]	R_{out} [mm]	E_s [GPa]	b_s [mm]
0.44	12.4	2.0	8
h_s [rad]	δ_s [mm]	R_s [mm]	θ_s [rad]
2	0.9	11	1.52

TABLE I
VALUES FOR CLUTCH CALCULATIONS.

In this way, controlling the applied load and monitoring the motor position, motor current, and string position continuously real-time were possible. It should be noted that while a motor encoder was present, it was not used in a feedback controller in order to better validate the models in Section III-C. Force and displacement characteristics in both winching and twisting phases, particularly during the transition between the two phases, were analyzed using data derived from the actuator's intrinsic parameters.

V. NUMERICAL MODEL CALCULATIONS

A. Friction Clutch Transition Torque

To determine how to set τ_{fr}, the desired load force trigger F was set to 30 N. From here, Equations 2, 3, and 4 were used to determine how much deflection to put into the cantilever friction contact. The values for the other variables can be found in Table I. The resulting rotational friction τ_{fr} was 0.011 N·m, and the relationship described in Equation 1 holds true for this design.

B. Triggering the Slip Clutch

For the reverse direction for when the gearbox dial hits the hard stop and unwinching begins, the torque that is applied when the clutch in the unidirectional bearing starts slipping was calculated to be 0.23 N·m using Table I and Equation 6. Additionally, the maximum motor torque of a 775 brushed motor is 0.79 N·m, and the antagonist force generated by the cylinder was set to approximately 30 N. With these values, it can be seen that the conditions in Equations 7 and 8 both hold true, so the reverse mechanism should perform as intended.

VI. PERFORMANCE ANALYSIS

A. Displacement Tests

To validate the actuator's capability to return to its initial state, a series of displacement tests were conducted. The string was initially wound around the winch, and the

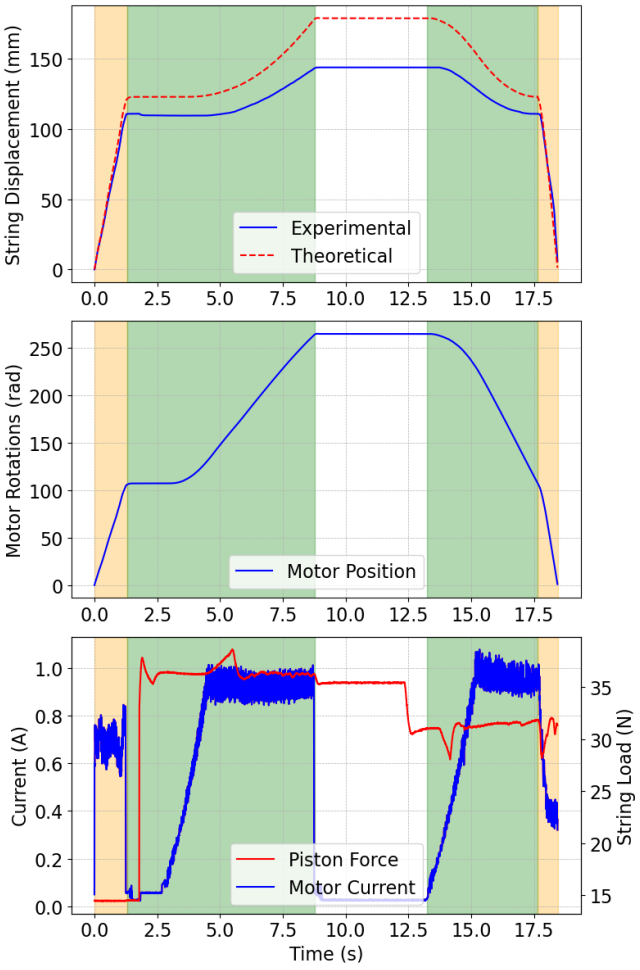

Fig. 8. Displacement over time for a full operation cycle. The first and second orange shaded regions represent the winching and unwinching phases. The first and second green shaded regions represent the twisting and untwisting phases. Note that the beginning of each phase comes with a sharp change in motor current, which can be used to track motor rotations for the winching phases.

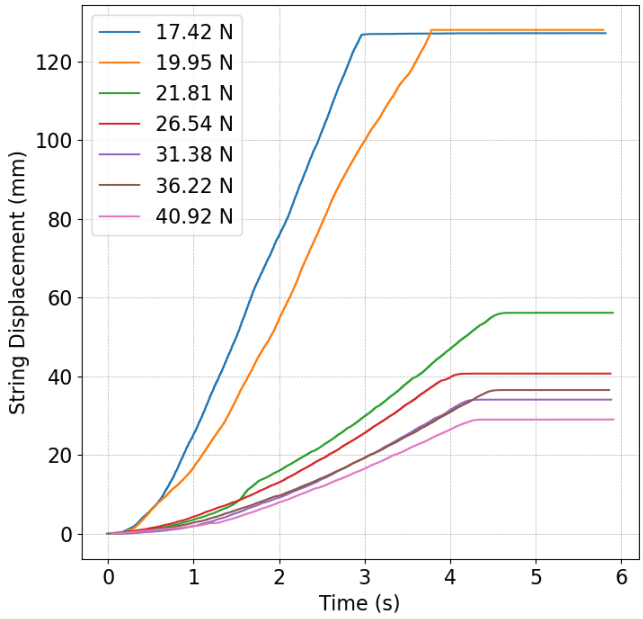

Fig. 9. Forward mechanism load force threshold testing. The forward mechanism was tested multiple times. Each line represents a single forward cycle under a different load applied to the end of the string, as indicated in the legend. It should be noted that around 31.38 N of applied load, the actuator appears to start purely twisting, suggesting that this is the approximate string load force threshold that triggers the transition from winch to twist. Additionally, the plateaus at the end of the displacement under 17.42 N and 19.95 N are due to the string fully extending the cylinder to the end of its stroke length rather than a commanded stop by the actuator.

pneumatic cylinder was positioned slightly beyond its fully retracted state to accommodate variations in the final position after unwinching. The operational cycle comprised of four phases: winching, twisting, untwisting, and unwinching. A 5-second pause between the twisting and untwisting phases facilitated clear demarcation of these stages. The applied string load for each phase is detailed in Fig. 8.

The experimental results, presented in Fig. 8, illustrate the displacement over time for each operational phase. Notably, error accumulates at each stage, as reflected by the deviation in the winching phase and the consequent discrepancy in the subsequent twisting displacement compared to the predicted trajectory. To accurately assess the models described in Equations 10 and 11, the relative error at the conclusion of the initial winching phase was subtracted from the theoretical twisting and untwisting phases. The relative error during the winching phases was determined to be 6.96 mm, while that during the twisting phases was 7.77 mm. These relatively low error values validate the string displacement equations, although they also highlight potential areas for refinement. It is plausible that these discrepancies are attributable to frictional losses within the transmission, which would reduce the actual winch velocity below the expected value.

Further analysis of the motor encoder data in relation to string position confirms the actuator's ability to closely return to its original state, with the string fully untwisted and unwinched. The start of the twisting phase (first green region in Fig. 8) is marked by the sharp dip in current, indicating reduced motor torque demand for pure twisting. From this point to the 5-second pause, the number of twists was recorded to be 157.59 radians. The end of the untwisting was marked by a similar change in current as the dial contacts the hard stop (end of the second green region in Fig. 8). The number of untwists was recorded to be 157.34 radians, demonstrating effective and nearly complete untwisting and validating the mechanical rotation tracking concept based on the gearbox dial. At the conclusion of the operation cycle when the motor encoder registered zero radians, the string displacement was measured at 5.87 mm, indicating a nearly complete unwinch as well as those frictional transmission losses mentioned earlier.

B. Clutch Torque Threshold

To verify the tuned torque threshold of the actuator achieved by adjusting the cantilever contact beam in accordance with Equations 1, 2, and 3, tests of the forward mechanism were conducted under varying load conditions. These

tests involved incrementally increasing the pressure within the cylinder for each test run and executing a single forward cycle. The resulting displacement data are presented in Fig. 9, where each line corresponds to the string displacement under the specific load indicated by the line color.

As depicted in Fig. 9, string displacement under pure twisting exhibits more pronounced exponential behavior, which is consistent with observations in Fig. 8 and prior research [8]. This was predicted when comparing the pure twisting Equation 11 to the more linear behavior described by the pure winching Equation 10. Due to the inherent design of this actuator, progressively increasing the string load leads to an increase in concurrent twisting while winching until all displacement is attributed completely to twisting. The force at this transition to pure twisting can be observed as the steady state position no longer decreases and the exponential behavior stays consistent despite increasing the string load. According to Fig. 9, this threshold is approximately 31 N, which aligns with the desired threshold of 30 N for which the actuator was designed (see Section V-A). The discrepancy between these values can be attributed to friction unaccounted for in the bearings and gearbox, which would increase τ_{fr} and consequently the force threshold.

VII. CONCLUSIONS AND FUTURE WORK

We have presented a novel single-motor actuator system that combines a twisted string actuator (TSA) with a winch mechanism. By integrating passive automatic clutches, the actuator seamlessly transitions between winching and twisting modes, achieving both high displacement and high force output. The proposed design eliminates the need for additional motors, simplifying the system while maintaining versatility.

Mathematical models were developed to describe the actuator's operation, including the torque and force output characteristics required for engagement of each clutch. Experimental validation demonstrated that the actuator's performance closely aligns with the theoretical predictions, verifying its ability to transition smoothly between modes and reliably return to its original state after operation. The results show that the hybrid TSA-winch actuator can be a compact, efficient, and adaptable solution for robots requiring rapid movement followed by significant force.

Future work will focus on refining the actuator to reduce friction losses and improve mechanical efficiency. Further miniaturization of the design presented here will make it suitable for applications in wearable robotics, tendon-driven robotic systems, and microscale actuators. Additionally, the scalability of this actuator will be investigated to assess its performance across a range of sizes and load conditions. Integrating the actuator into practical systems, such as robotic grippers and exoskeletons, will validate its potential in real-world scenarios. Ultimately, this work represents an advancement in the field of robotic actuators by combining the strengths of winching and twisting mechanisms into a single, efficient solution.

REFERENCES

[1] M. Shoham, "Twisting Wire Actuator," *Journal of Mechanical Design*, vol. 127, no. 3, pp. 441–445, Jul. 2004. [Online]. Available: https://doi.org/10.1115/1.1866156

[2] T. Würtz, C. May, B. Holz, C. Natale, G. Palli, and C. Melchiorri, "The twisted string actuation system: Modeling and control," in *2010 IEEE/ASME International Conference on Advanced Intelligent Mechatronics*. IEEE, 2010, pp. 1215–1220. [Online]. Available: https://ieeexplore.ieee.org/abstract/document/5695720/

[3] S. H. Jeong and K.-S. Kim, "A 2-Speed Small Transmission Mechanism Based on Twisted String Actuation and a Dog Clutch," *IEEE Robotics and Automation Letters*, vol. 3, no. 3, pp. 1338–1345, Jul. 2018, conference Name: IEEE Robotics and Automation Letters. [Online]. Available: https://ieeexplore.ieee.org/document/8253814/?arnumber=8253814

[4] K. W. O'Brien, A. Xu, D. J. Levine, C. A. Aubin, H.-J. Yang, M. F. Xiao, L. W. Wiesner, and R. F. Shepherd, "Elastomeric passive transmission for autonomous force-velocity adaptation applied to 3D-printed prosthetics," *Science Robotics*, vol. 3, no. 23, p. eaau5543, Oct. 2018, publisher: American Association for the Advancement of Science. [Online]. Available: https://www.science.org/doi/10.1126/scirobotics.aau5543

[5] Y. J. Shin, H. J. Lee, K.-S. Kim, and S. Kim, "A Robot Finger Design Using a Dual-Mode Twisting Mechanism to Achieve High-Speed Motion and Large Grasping Force," *IEEE Transactions on Robotics*, vol. 28, no. 6, pp. 1398–1405, Dec. 2012.

[6] S. Kim, J. Sim, and J. Park, "Elastomeric continuously variable transmission combined with twisted string actuator," *IEEE Robotics and Automation Letters*, vol. 5, no. 4, pp. 5477–5484, 2020, publisher: IEEE. [Online]. Available: https://ieeexplore.ieee.org/abstract/document/9137664/

[7] T. Tsabedze, R. Konda, D. Bombara, and J. Zhang, "Model-Based Performance Analysis of Twisted String Actuators With Comparison to Spooled Motor Tendon-Driven Actuators," *IEEE Robotics and Automation Letters*, vol. 9, no. 9, pp. 7739–7746, Sep. 2024, conference Name: IEEE Robotics and Automation Letters. [Online]. Available: https://ieeexplore.ieee.org/document/10607867/?arnumber=10607867

[8] R. Poon, V. Padia, and I. W. Hunter, "A Novel Twisted-Winching String Actuator for Robotic Applications: Design and Validation," Oct. 2024, arXiv:2410.12097. [Online]. Available: http://arxiv.org/abs/2410.12097

[9] Seok Hwan Jeong, Y. J. Shin, K.-S. Kim, and S. Kim, "Dual-mode twisting actuation mechanism with an active clutch for active mode-change and simple relaxation process," in *2015 IEEE/RSJ International Conference on Intelligent Robots and Systems (IROS)*. Hamburg, Germany: IEEE, Sep. 2015, pp. 5832–5837. [Online]. Available: http://ieeexplore.ieee.org/document/7354205/

[10] S. H. Jeong, K.-S. Kim, and S. Kim, "Control of and experimentation on an active dual-mode twisted string actuation mechanism," in *2017 IEEE International Conference on Advanced Intelligent Mechatronics (AIM)*, Jul. 2017, pp. 987–992, iSSN: 2159-6255. [Online]. Available: https://ieeexplore.ieee.org/document/8014147/?arnumber=8014147

[11] S. Jeong, Y. Lee, and K.-S. Kim, "Applications: Twisted String Actuation-based Compact Automatic Transmission," *2021 IEEE International Conference on Robotics and Automation (ICRA)*, pp. 10 870–10 876, May 2021, conference Name: 2021 IEEE International Conference on Robotics and Automation (ICRA) ISBN: 9781728190778 Place: Xi'an, China Publisher: IEEE. [Online]. Available: https://ieeexplore.ieee.org/document/9561453/

[12] S. H. Jeong, Y. J. Shin, and K.-S. Kim, "Design and Analysis of the Active Dual-Mode Twisting Actuation Mechanism," *IEEE/ASME Transactions on Mechatronics*, vol. 22, no. 6, pp. 2790–2801, Dec. 2017. [Online]. Available: http://ieeexplore.ieee.org/document/8089392/

[13] Z. Lu, R. Wang, Y. Xiao, T. Liu, C. Liu, and H. Zhao, "A load-adaptive hoisting mechanism based on spring-loaded rope and variable radius reel," *Advanced Robotics*, vol. 37, no. 23, pp. 1520–1531, Dec. 2023, publisher: Taylor & Francis _eprint: https://doi.org/10.1080/01691864.2023.2285802. [Online]. Available: https://doi.org/10.1080/01691864.2023.2285802

[14] M. Phlernjai, T. Takayama, and T. Omata, "Passively switched cable-driven transmission for high-speed/high-force robot finger," *Advanced Robotics*, vol. 30, no. 24, pp. 1559–1570, Dec. 2016, publisher: Taylor & Francis _eprint: https://doi.org/10.1080/01691864.2016.1251336. [Online]. Available: https://doi.org/10.1080/01691864.2016.1251336